Sensing Single Mixed-Monolayer Protected Gold Nanoparticles by the α-Hemolysin Nanopore

ARTICLE *in* ANALYTICAL CHEMISTRY · SEPTEMBER 2013

Impact Factor: 5.64 · DOI: 10.1021/ac4014836 · Source: PubMed

6 AUTHORS, INCLUDING:

Elisa Campos
University of Coimbra
15 PUBLICATIONS **76** CITATIONS
SEE PROFILE

Colin E. McVey
New University of Lisbon
24 PUBLICATIONS **568** CITATIONS
SEE PROFILE

Francesco Stellacci
École Polytechnique Fédérale de Lausanne
192 PUBLICATIONS **7,177** CITATIONS
SEE PROFILE

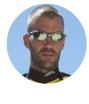

James Robert Yates
New University of Lisbon
13 PUBLICATIONS **442** CITATIONS
SEE PROFILE

analytical chemistry

Article

pubs.acs.org/ac

Sensing Single Mixed-Monolayer Protected Gold Nanoparticles by the α-Hemolysin Nanopore

Elisa Campos,*[,†] Colin E. McVey,[‡] Randy P. Carney,[§] Francesco Stellacci,[§] Yann Astier,[†,∥] and James Yates[†]

[†]Single Molecule Processes Laboratory, Instituto de Tecnologia Química e Biológica, Universidade Nova de Lisboa, Av. da República, 2780-157 Oeiras, Portugal

[‡]Structural Genomics Laboratory, Instituto de Tecnologia Química e Biológica, Universidade Nova de Lisboa, Av. da República, 2780-157 Oeiras, Portugal

[§]Institute of Materials, École Polytechnique Fédérale de Lausanne, EPFL-STI-IMX-SuNMIL Station 12, Lausanne, CH-1015, Switzerland

Supporting Information

ABSTRACT: Gold nanoparticles are widely used in various applications in fields including chemistry, engineering, biology, medicine, and electronics. These materials can be synthesized and modified with ligands containing different functional groups. Among nanoparticles' characteristics, chemical surface composition is likely to be a crucial feature, demanding robust analytical methodologies for its assessment. Single molecule analysis using the biological nanopores α-hemolysin and its E111A mutant is presented here as a promising methodology to stochastically sense organic monolayer protected gold-nanoparticles with different ligand shell compositions. By monitoring the ionic current across a single protein nanopore, differences in the physical and chemical characteristics (e.g., size, ligand shell composition, and arrangement) of individual nanoparticles can be distinguished based on the differences in the current blockade events that they cause. Such differences are observed in the spread of both the amplitude and duration of current blockades. These values cannot be correlated with a single physical characteristic. Instead the spread represents a measure of heterogeneity within the nanoparticle population. While our results compare favorably with the more traditional analytical methodologies, further work will be required to improve the accuracy of identification of the NPs and understand the spread of values within a nanoparticle preparation as well as the overlap between similar preparations.

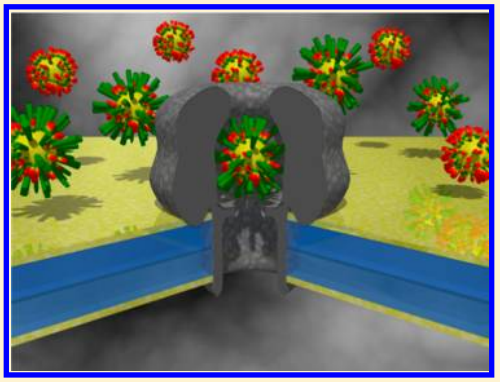

Stochastic sensors based on nanopores, both biological and synthetic, are currently under intense investigation.[1−4] Nanopore-based techniques are being developed for use in the fields of single-molecule detection of metal ions,[5] explosives,[6] chemical warfare agents,[7] organic molecules,[8] amino acid enantiomers,[9] peptides,[10] proteins,[11] microRNAs,[12] reactive molecules,[13] and most prominently in DNA sequencing.[14] Among biological nanopores, the transmembrane nanopore α-hemolysin (αHL; Figure 1A) has been widely studied and applied in sensing applications.[11−15,16] This protein presents remarkable stability under extreme conditions of pH (i.e., from 4 to 11),[17] transmembrane potential (up to 160 mV),[18] temperature (0−95 °C),[19] salt concentration (0.1−4.0 M KCl),[20] and chemical denaturants (e.g., up to 7.2 M urea).[21] In addition, it has recently been shown that ionic liquids may also be used as electrolytes, replacing the commonly used, buffered, NaCl/KCl solutions. Use of ionic liquids can enhance resolution of blockade events and may also permit the analysis of ions and molecules that are insoluble in water or whose detection is affected by NaCl/KCl.[22]

Analysis of the αHL heptamer structure (PDB accession code 7AHL) suggested that the central constriction (1.4 nm in diameter) would be of particular importance to sensing applications. This constriction is formed by the side chains of the ion pair Glu111 and Lys147.[23] The αHL nanopore can be engineered,[24] via site-directed mutagenesis, with atomic precision, using its high resolution crystal structure as a guide.[23] In a recent study, we engineered an αHL-E111A (hereafter mentioned E111A, for simplicity) mutant protein nanopore in which the Glu111 residue is replaced with an alanine, thus preventing Glu111-Lys147 interactions and facilitating electrostatic interactions between Lys147 and single sulfonate-terminated monolayer-protected coated nanoparticles (nanoparticle, NP). A comparison between the wild-type (WT-αHL) and the E111A mutant revealed that single sulfonate-terminated monolayer-protected NPs are captured in the

Received: May 16, 2013
Accepted: September 22, 2013
Published: September 23, 2013

dx.doi.org/10.1021/ac4014836 | Anal. Chem. 2013, 85, 10149−10158

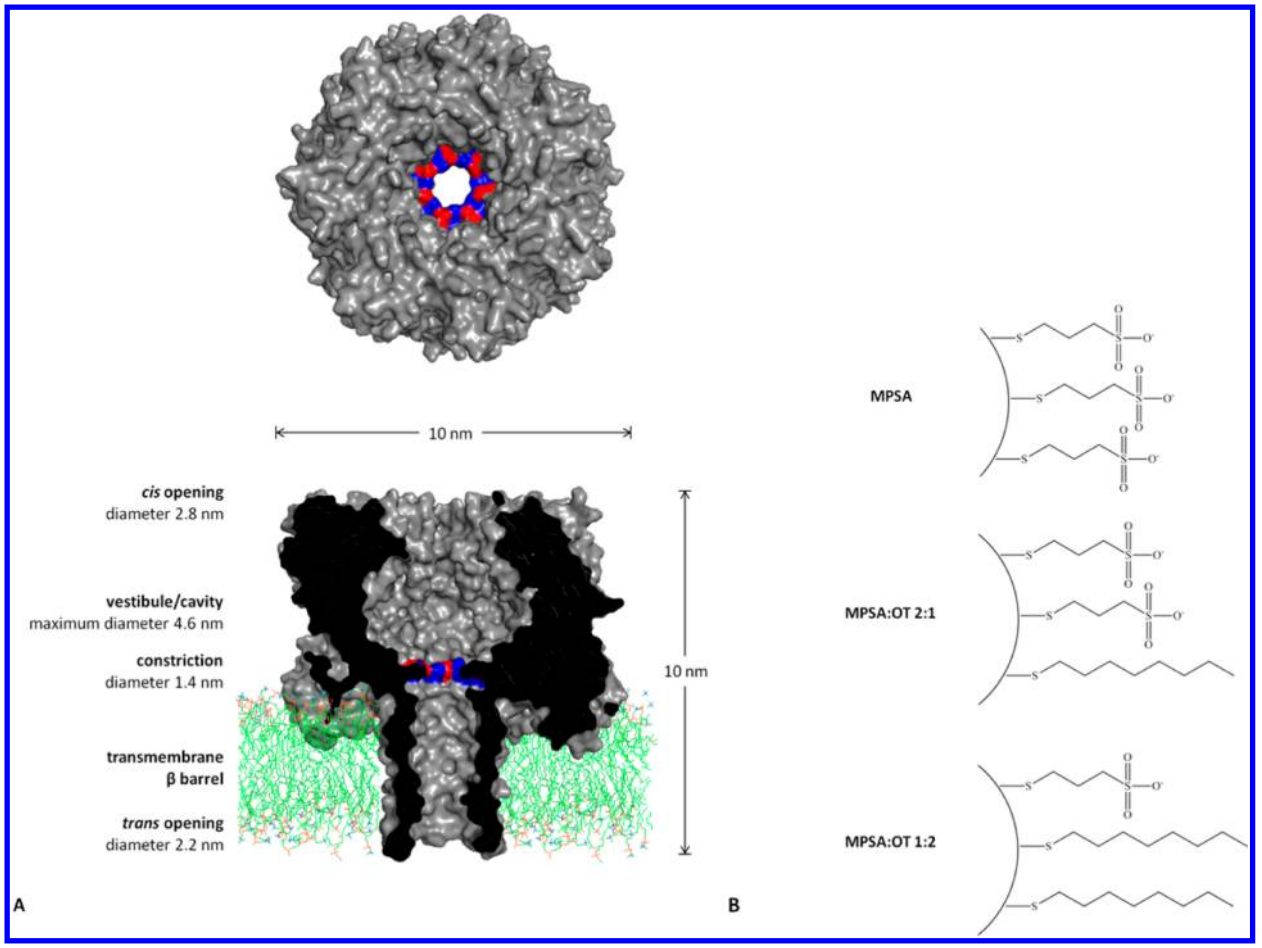

Figure 1. Molecular models of the (A) Staphylococcal wild-type α-hemolysin protein nanopore: a top view and a cross-sectional view of the mushroom-shaped heptamer (rendered from PDB accession code 7AHL using PyMOL software[38])[23,39] are shown in surface form (gray). The positions of the ion pairs, Glu111-Lys147 at the constriction region, are colored in red and blue, respectively; (B) ligand shell composition of the nanoparticles used in this study; structures were rendered by ChemBioDraw Ultra 12.0 software (CambridgeSoft).

nanopore's cavity via electrostatic interactions with Lys147 residues in the constriction region.[25]

Organic monolayer protected NPs are promising materials for a wide range of applications in fields including chemistry, engineering, biology, medicine[26−28] and electronics.[29] NPs have unique properties that depend upon their size and their composition. Currently, the determination of their properties is based on measuring bulk averages.[30] Here, we introduce an alternative and promising protein nanopore-based method that allows for the characterization of individual NPs. Despite the fragility of the synthetic planar lipid bilayer in which nanopores are formed, there is precedence for using biological nanopores for high-throughput sensing applications.[31−34] Therefore, we used our previous[25] study as a basis for applying WT-αHL and E111A mutant nanopores to the study of mixed-monolayer protected gold NPs. Since a NP's dimensions are in same range of the dimensions of a single pore (~3−4 nm), it offers the possibility of characterizing ligand shell composition on a single-particle basis.

In this study, we focused on a ligand shell composition based upon charged sulfonate terminated alkanethiol ligands mixed with nonpolar methyl terminated alkanethiol ligands. Similar combinations have already been applied to model surfaces to study the effects of surface characteristics upon biological responses, namely, platelet adhesion.[35,36] Three types of water-soluble NPs were synthesized and studied (Figure 1B). The first type of NP was coated with just a single type of the hydrophilic ligand 3-mercapto-1-propanesulfonate (MPSA), to generate MPSA NPs. The other two types of NPs were coated with alternating domains of hydrophilic (MPSA) and hydrophobic 1-octanethiol (OT) ligands in different molar ratios of 2:1 and 2:1 (hereafter referred to as MPSA:OT 2:1 NPs and MPSA:OT 1:2 NPs, respectively). For these experiments, a single protein nanopore was inserted in a planar lipid bilayer that separates two compartments (henceforth called cis and trans) containing an aqueous electrolyte. By applying an electrical potential, in the millivolt range, across the bilayer, an ionic current flowing through the nanopore can be measured. The interaction of a NP with the nanopore modulates the ionic current.[37] We show that it was possible to detect differences in the NPs' ligand shell composition via changes in the level of ionic current and the duration of these current changes that occur when the electric field-driven NPs interact with the nanopore.

EXPERIMENTAL SECTION

Materials. All reagents used were purchased from Sigma-Aldrich (Sigma-Aldrich, St. Louis, MO), unless otherwise stated, and were used as received.

Genetic Construct and Mutagenesis. The E111A mutant was constructed by site-directed mutagenesis, as previously described.[25]

dx.doi.org/10.1021/ac4014836 | Anal. Chem. 2013, 85, 10149−10158

Expression and Purification of E111A Mutant. The E111A mutant was expressed as described elsewhere.[25] *Escherichia coli* BL21 (DE3) cells (Novagen, EMD Chemicals, Gibbstown, NJ) containing the plasmid pT7-αHL-E111A were harvested and chemically lysed as described previously.[25] Following cell pellet lysis, the supernatant containing the αHL-E111A monomer was first fractionated with ammonium sulfate (AS), at 4 °C.[40] E111A protein that precipitated between 40 and 45% AS was recovered by centrifugation at 29 000*g* for 30 min, at 4 °C, and resuspended in 20 mM HEPES (pH 7.0) containing 20 mM NaCl. The solution was dialyzed against the same buffer, 3× 2 h at 4 °C, in a Slide-A-Lyzer G2 dialysis cassette (3.5 kDa MWCO; Thermo Scientific, Waltham, MA). The suspension was centrifuged at 29 000*g* for 20 min, at 4 °C, and the clear supernatant was loaded onto a strong cation-exchange HiTrap SP Sepharose XL column (GE Healthcare, Buckinghamshire, U.K.) attached to an ÄKTA Explorer system (GE Healthcare, Buckinghamshire, U.K.) and pre-equilibrated in the previous buffer. All purification procedures were carried out at room temperature. The protein was eluted with a linear salt gradient from 20 mM to 2 M NaCl in 20 mM HEPES (pH 7.0). The fractions containing the purified protein were analyzed by sodium dodecyl sulfate-polyacrylamide gel electrophoresis (SDS-PAGE) with the Coomassie Blue staining method. The resulting samples were stored frozen in aliquots with the addition of 10% glycerol at −80 °C.

MPSA- and MPSA:OT 1:2 Gold NPs Synthesis. The NPs were synthesized with the one-phase Brust method.[41,42] This method has the advantage of producing NPs whose ligand shell composition typically matches the stoichiometric ratio of ligands used during the synthesis.[43] Briefly, 0.9 mmol of $HAuCl_4$ was dissolved in 150 mL of ethanol (all solvents used had been previously purged with N_2 for at least 1 h) in a clean (by aqua regia solution) round-bottom flask. In total, 0.75 mmol of the desired molar ratio of ligands (MPSA and OT, for details see Figure 1B) for each particular batch of particles was mixed in 10 mL of methanol (which is a better solvent than ethanol for sulfonate ligands) and added to the stirring gold solution. After 5 min, 150 mL of a saturated reducing solution of $NaBH_4$ was added dropwise to the reaction vessel, initiating a drastic color change from yellow to reddish-brown. The reaction was left to stir for 2 more hours before being placed at 4 °C overnight in order to precipitate the particles. The supernatant was removed, and the particles were cleaned of impurities and byproducts through centrifugation in acetone, ethanol, and methanol. The pelleted particles were dried thoroughly and used within a few months of synthesis.

MPSA- and MPSA:OT 1:2 Gold NPs Characterization. Analytical ultracentrifugation (AUC) was used to determine NPs size distribution, following a method previously developed to find the hydrodynamic diameter and density distributions of monolayer protected NPs.[44] Additionally, ^{1}H NMR analysis was used to confirm that the actual molar ratio of ligands on the surface of the particles was close to the synthetic one. For this procedure, 30 mg of NPs and 25 mg of KCN were dissolved in 1 mL of MeOD (deuterated methanol-*d*4, chosen because it solubilizes both OT and MPSA) and sonicated for 4 h, during which time the gold core dissolved and precipitated. The resulting solution contained only free ligands that were previously coating the particles' surfaces. Immediately prior to ^{1}H NMR analysis, this solution was filtered through a 0.2 μm membrane filter, to remove the gold and other insolubilities. This data is presented in Table S-1 in the Supporting Information.

Single-Channel Current Recordings. Planar lipid bilayers were formed by the lipid monolayer folding technique.[45] The cis and trans compartments of the chamber (NanoPore Solutions, Portugal) were separated by a 50-μm-thick Teflon film (Goodfellow Cambridge Ltd., Huntingdon, U.K.) containing a 100- to 150-μm diameter orifice. The aperture was pretreated with 10% v/v hexadecane in *n*-pentane. 1,2-Diphytanoyl-*sn*-glycero-3-phosphocholine (Avanti Polar Lipids, Alabaster, AL) in *n*-pentane (10 mg mL^{-1}) was added to both compartments, filled previously with electrolyte solution containing 2 M KCl and 10 mM HEPES (pH 8.0). After evaporation of *n*-pentane, the lipid bilayer was formed by lowering and raising the electrolyte level in one or both sides of the aperture. Monomeric WT-αHL and E111A mutant were added to the cis compartment from a stock solution made in distilled water (according to supplier instructions) or in storage buffer (20 mM HEPES, 350 mM NaCl, pH 7.0, 10% v/v glycerol), respectively. In this way, the protein nanopore presented its mushroom cap facing the cis compartment, while the β-barrel was spanning the lipid bilayer, facing the trans compartment of the chamber. After a single protein nanopore was formed in the lipid bilayer, NPs were added to the cis compartment at a final concentration of 10 μg mL^{-1}. Positive potentials of +40, +60, +80, and +100 mV were applied across the lipid bilayer with Ag/AgCl electrodes. The cis compartment was grounded so that a positive potential indicates a higher potential in the trans compartment, meaning that positive charges are moving from the trans to cis side of the lipid bilayer. External electrical noise was shielded using a Clutch faraday cage (NanoPore Solutions, Portugal), inside which the bilayer recording amplifying headstage, chamber, and electrodes were enclosed. Current changes reflecting NPs interactions with the protein nanopore were recorded using a patch clamp amplifier (EPC8, HEKA Elektronik, Lambrecht/Pfalz, Germany), in the whole-cell mode, and filtered at a cutoff frequency of 5 kHz using a built-in 7-pole low-pass Bessel filter. The data were acquired by using PatchMaster software (HEKA Elektronik, Lambrecht/Pfalz, Germany), by a computer coupled to a LIH 8 + 8 A/D converter (HEKA Elektronik, Lambrecht/Pfalz, Germany) equipped with a 16-bit acquisition board, at a sampling frequency of 10 kHz. All measurements were performed at room temperature. A video showing the main steps of this protocol can be found at www.nanoporesolutions.com (under the Resources tab).

Data Analysis. Current traces were analyzed with pCLAMP 10.3 software (Molecular Devices, Sunnyvale, CA). The interaction events were detected manually using the single-channel search tool in pCLAMP 10.3. For analysis, current traces were digitally filtered with a Bessel (8-pole) lowpass filter with pCLAMP 10.3 software, at −3 dB cutoff frequency of 1000 Hz or at 200 Hz (in the case of the intrablockade events), assuming that the cutoff frequency must be larger than 0.01 times the sampling frequency.[46] The filtering cutoff frequency (f_c) affects the resolution of the threshold detection method: a Bessel filter with a cutoff frequency of 5 kHz is characterized by a filter rise time (t_r, given by $0.3321/f_c$) of 0.066 ms.[47] In order to measure dwell times, the duration of events needs to be above roughly $1.3t_r$ (before errors become negligible), which corresponds to a duration of 0.086 ms, when filtering at 5 kHz.[47] The event duration must also have a duration of at least $2t_r$ (i.e., 0.133 ms in this study) before its amplitude can be

dx.doi.org/10.1021/ac4014836 | *Anal. Chem.* 2013, 85, 10149−10158

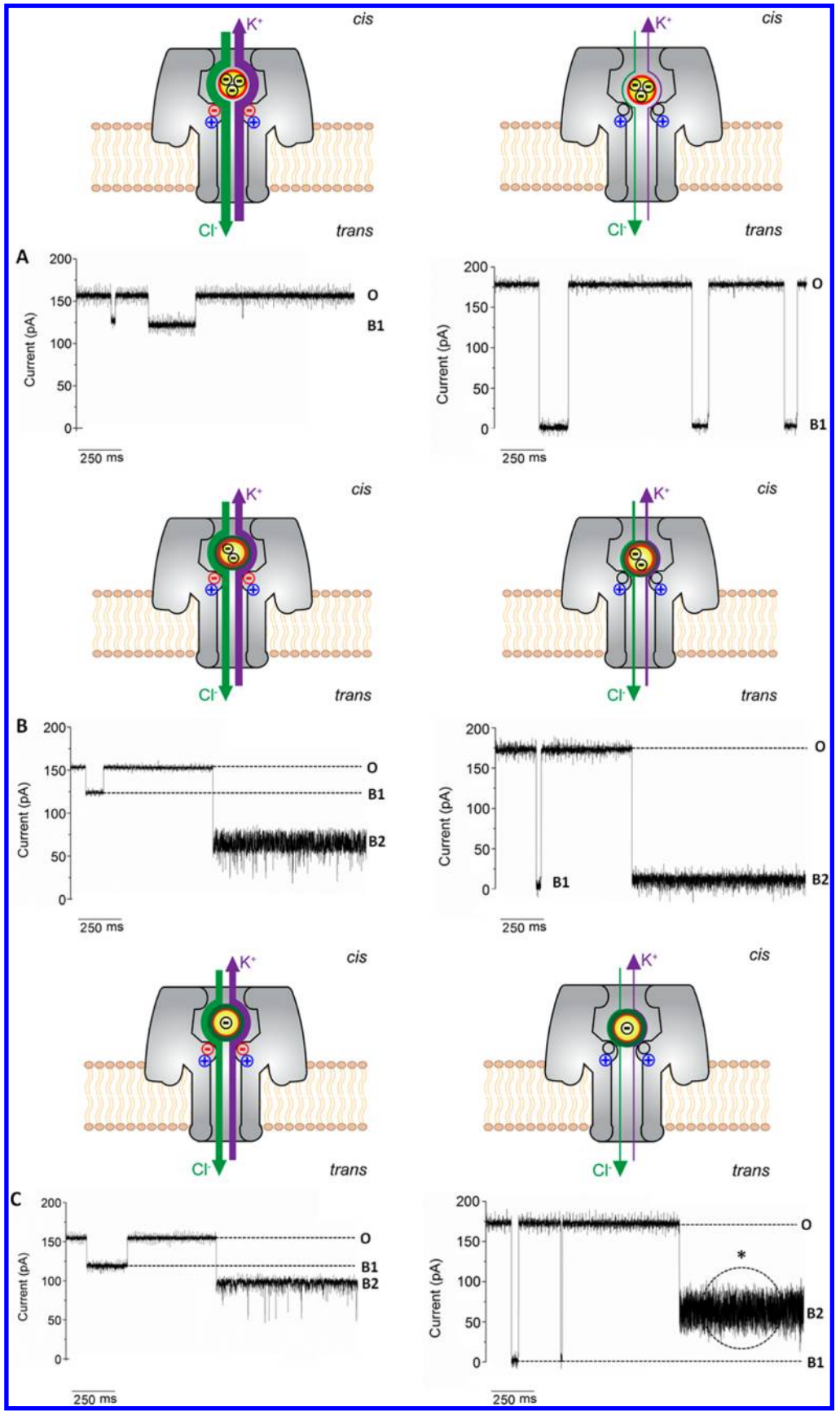

Figure 2. continued

dx.doi.org/10.1021/ac4014836 | *Anal. Chem.* 2013, 85, 10149−10158

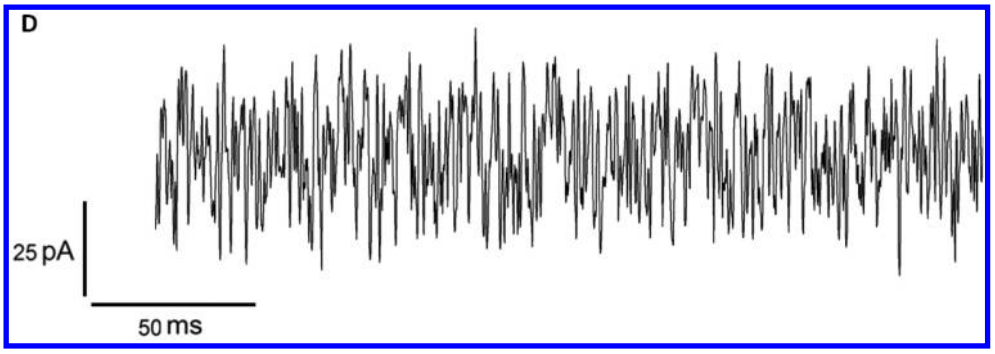

Figure 2. Representative current traces from single channel recordings of single (A) MPSA, (B) MPSA:OT 2:1, and (C) MPSA:OT 1:2 NPs interacting with (left side) WT-αHL and (right side) E111A mutant protein nanopores. Open (denoted by O) and blocked (denoted by B) pore states denote the electrical response of the nanopore before and while interacting with a single NP. Typical transient (denoted by B1) and longer (denoted by B2) current blockades where a single NP is lodged within the protein nanopore are shown. (D) The magnified region of the trace highlighted by $*$. Cartoons above each trace illustrate the influence of the NP−nanopore interactions on the time-average ionic current, under A positive applied transmembrane potential. Highlighted for the WT-αHL nanopore (gray) are Glu111 (negatively charged; red) and Lys147 (positively charged; blue) in the constriction region. For the E111A mutant nanopore (gray) Glu111Ala (uncharged; black) and Lys147 (positively charged; blue) are highlighted in the constriction region. A single NP is represented inside the nanopore cavity, showing its gold-core (yellow) and the ligands MPSA (red layer) and OT (green layer). The thickness of these layers is an attempt to convey the content of the ligand shell. The relative (expected) charged on the NP is represented by $\ominus$. The relative residual K^+-Cl^- ionic current is represented by the thickness of purple and green arrows, respectively. NPs (10 μg mL^{-1}) were added to the cis chamber. The data was recorded at +80 mV in 2 M KCl, 10 mM HEPES, pH 8.0.

measured reliably.[47] For practical analysis, the limit for measurement of durations was set to 1 ms. The events shorter than those limits were excluded when fitting the distribution histograms. Each event arising from interaction of a NP with the protein nanopore can be characterized by two parameters, namely, the ionic current blockade (or the change in current amplitude) and the blockade duration (dwell time). Accordingly, a convenient method to view the data is via a two-dimensional scatter plot coupled to marginal histograms.[48] In order to describe the data, one needs to assign a value or measure to the central tendency (or central location) and to include a measure of spread or dispersion (which describes the variability in the sample). When dealing with skewed and/or data with outliers, as in the present study, the median and interquartile range are often reported as the best choice of measure of central tendency and spread, respectively, because these measures are not strongly affected by the skewed values or outliers. Here, the interquartile range is the difference between the first and the third quartile (also called the 25th and the 75th percentile, respectively).[49,50] Therefore data were also graphically depicted as box plots, displaying the median, the upper (third) and lower (first) quartiles, and the minimum and maximum data values.[51] For display, current traces were digitally filtered with a Bessel (8-pole) lowpass filter with pCLAMP 10.3 software, at −3 dB cutoff frequency of 800 Hz or at 200 Hz (in the case of the intrablockade events). Then, full sweeps were exported as ABF files and imported into OriginPro 8 SR4 (OriginLab Corporation, Northampton, MA). Figures depicting current traces and graphical representations of data were made with OriginPro 8 SR4 (OriginLab Corporation, Northampton, MA) and Microsoft Office Excel (2007) software, respectively. Data were collected in 2−3 independent experiments/pores involving >3 recordings each.

Molecular Graphics. The models of αHL were generated from a .pdb file (PDB accession code 7AHL) using PyMOL.[38]

RESULTS AND DISCUSSION

In order to study the interactions of the ligand shell with the WT-αHL and E111A mutant protein nanopores, we used three different types of organic monolayer protected NPs consisting of an inorganic gold core coated with thiolated organic molecules: MPSA, MPSA:OT 2:1, and MPSA:OT 1:2. According to bulk analysis methods, all types of NPs studied here had similar core sizes, differing only in the composition of their ligand shells (see the Supporting Information, for details, in particular Tables S-1 and S-2). The hydrodynamic diameters of MPSA:OT 2:1 and MPSA:OT 1:2 NPs were estimated, by AUC, to be between 3.90 and 7.52 nm. MPSA NPs were estimated to be slightly smaller with a hydrodynamic diameter between 3.90 and 6.21 nm (Supporting Information, Table S-2). The αHL protein nanopore cis opening diameter (2.8 nm; Figure 1A), restricts the size of the NPs that are able to enter and interact with the cavity.[52] At first, it may appear counterintuitive that NPs are able to enter the cavity at all. However, we assume that the diameter estimated by AUC includes a small hydration shell and also that the ligands possess a degree of flexibility and, thus, can be bent or compressed. We also assume that the interactions recorded throughout this study have occurred within the nanopore cavity and that the interactions at the mouth of the nanopore (if they occur) are invisible or not accurately measured at our recording resolution. The same assumption was made before[53] and considered that transient collisions of DNA with the mouth of the αHL nanopore would cause events shorter than 10 μs and were thus ignored in the analysis.

The WT-αHL and E111A mutant protein nanopores undergo stochastic interactions with all three types of NPs, at pH 8.0 (Figure 2).

Typically, events displaying two very different profiles are observed: (i) transient current blockades of up to 30% of the open pore current (Figure 2, labeled "B1") which correspond to NP-nanopore interactions where the NP is able to enter into the nanopore and then exit from the nanopore and (ii) indefinitely long or permanent current blockades of greater than 30% of the open pore current (Figure 2, labeled "B2"), which correspond to NP−nanopore interactions where the NP is able to enter into the nanopore cavity but is unable to exit. The interpretation that the longer blockade events would correspond to capture events within the αHL cavity, while the shorter events correspond to interactions with the opening of

dx.doi.org/10.1021/ac4014836 | Anal. Chem. 2013, 85, 10149−10158

the nanopore, could be made. However, the results presented in this paper, and in a previous publication,[25] demonstrate that all recorded events occur within the αHL cavity. The logic for this statement is as follows: If interactions at both the opening and inside the nanopore are observed for the WT-αHL, when using the E111A mutant (or when changing the pH from 8.0 to 2.8), no effect (or at least a greatly reduced effect) would be observed on the interactions at the opening of the nanopore. A significant effect (shift) would only be observed for the interactions that occur within the cavity. The fact that replacing the WT-αHL with the E111A mutant or changing the pH from 8.0 to 2.8 influences the blockade level and dwell time of all interactions suggests that all of the interactions observed are occurring inside the nanopore cavity.

While with preparations of MPSA NPs only the first type of event is observed, with both compositions of MPSA/OT NP preparations both types of event are recorded. The transient current blockades allow for a distinction to be made between MPSA and MPSA/OT NPs, based on bulk differences in the ionic current signal (i.e., the median and the interquartile range, Table 1 and the Supporting Information, Figures S-2–S-4).

Table 1. Summary of the NPs Transient Capture Events in a Single WT-αHL and E111A Nanopore[a]

	WT-αHL			E111A		
	current blockade (%)	τ_{off} (s)	N	current blockade (%)	τ_{off} (s)	N
+40 mV						
MPSA	n.r.	n.r.	n.r.	99.1	0.816	114
MPSA:OT 2:1	n.r.	n.r.	n.r.	88.3	0.232	23
+60 mV						
MPSA	19.5	0.009	109	97.5	0.412	51
MPSA:OT 2:1	22.9	0.165	15	95.5	0.123	29
MPSA:OT 1:2	25.7	0.173	7	97.5	0.064	12
+80 mV						
MPSA	17.7	0.008	276	98.0	0.220	68
MPSA:OT 2:1	22.4	0.351	35	95.8	0.023	16
MPSA:OT 1:2	24.2	1.100	37	98.4	0.041	11
+100 mV						
MPSA	18.8	0.053	75	98.0	0.036	79
MPSA:OT 2:1	26.5	1.309	12	93.9	0.012	7
MPSA:OT 1:2	23.8	0.966	23	95.6	0.014	2

[a]Experiments were performed at applied potentials of +40 mV, +60 mV, +80 mV, and +100 mV in 2 M KCl, 10 mM HEPES (pH 8.0), in the presence of cis-side-added NPs, at a concentration of 10 μg mL^{-1}. Current blockade percentage = 100 × $(I_O - I_B)/I_O$, where I_O is the current of the open pore and I_B is the current of the blocked pore. Current blockade and dwell time (τ_{off}) values are the median of N events.[49,50] n.r., no NP capture events were recorded under these conditions.

Another apparent difference is that capture events are more frequent with MPSA NPs than with MPSA/OT NPs (see values for N in Table 1).

It is important to note that two types of analysis can be performed when analyzing nanopore data. Binding events are stochastic processes, both in terms of blockade level and dwell time. Traditionally data relating to blockade levels and dwell times are binned and presented as histograms. This generally results in a distribution of values around the mean. Blockade levels and dwell times can be thus presented as a mean, median, or mode along with a measure of the dispersion or spread. Here, results are presented as the median and interquartile range to better reflect the distribution of the underlying measurements. This could be considered as a bulk analysis (see the following section). However, it is also possible to consider each individual event and to try to assign individual NPs to a preparation based upon an individual blockade level or dwell time values (see later).

To summarize the "bulk" data observed, MPSA NPs captured by the WT-αHL protein nanopore cause lower current blockades and display shorter dwell times than captured MPSA/OT NPs. Interestingly, the spread of current blockade values observed for MPSA is lower than for MPSA/OT NPs (Supporting Information, Figure S-3). The interactions of MPSA and MPSA/OT NPs with the E111A mutant result in similar current blockades. However, the dwell time of the MPSA NPs in the E111A mutant is longer than the dwell time of MPSA/OT NPs.

We observe that MPSA NP capture events by WT-αHL, at all transmembrane potentials, result in current blockades with amplitudes between 17% and 21%, whereas MPSA:OT 2:1 and MPSA:OT 1:2 NP capture events lead to blockades of between 20% and 28% and between 21% and 29%, respectively. Concerning capture events by the E111A mutant, we see that MPSA NPs cause current blockades of 93% to 100%, at all tested transmembrane potentials, while MPSA:OT 2:1 NPs reduce the ionic current by 83% to 98% and MPSA:OT 1:2 NPs reduce the ionic current by 93% to 99% (Supporting Information, Figure S-3). A voltage threshold seems to exist since NP capture events are only observed at transmembrane potentials above +60 mV, for the WT-αHL, and above +40 mV, for the E111A mutant (except for MPSA:OT 1:2 where the voltage threshold is +60 mV). Table 1 also shows dwell time values for NP capture events by WT-αHL and by the E111A mutant at applied transmembrane potentials of +40, +60, +80, and +100 mV. When using the WT-αHL nanopore, we observe an increase in median dwell time with applied potential for all types of NPs. In fact, dwell time increases from 0.009 to 0.053 s, from 0.165 to 1.309 s, and from 0.173 to 0.966 s, during the capture events of MPSA, MPSA:OT 2:1, and MPSA:OT 1:2 NPs, respectively, when the applied potential is increased from +60 mV to +100 mV. The dwell time of NPs in the E111A mutant nanopore appears to decrease with increasing the applied transmembrane potential. We observe that dwell time decreases from 0.816 to 0.036 s, from 0.232 to 0.012 s, and from 0.064 to 0.014 s, during the capture events of MPSA, MPSA:OT 2:1, and MPSA:OT 1:2 NPs, respectively, when the applied potential increases from +40 to +100 mV (except for MPSA:OT 1:2 where the range is +60 to +100 mV).

We have previously postulated that the interaction between the NPs and the protein nanopore depends on the electrostatic interaction between Lys147 and the MPSA ligand. The interaction of MPSA NPs with the WT-αHL nanopore is weak, since Lys147 is mainly engaged in electrostatic interactions with Glu111. Conversely, in the E111A mutant nanopore, Lys147 is not able to engage in electrostatic interactions with the replacement alanine and, thus, the interaction of MPSA NPs with the residues of the constriction region is stronger and results in a near full blockade (Supporting Information, Figure S-1, top panel).[25] It was anticipated that, due to steric hindrance resulting from the higher content of the longer OT ligand, the MPSA/OT NPs would be less likely to form electrostatic interactions with Lys147. However the interaction between the MPSA/OT NPs

dx.doi.org/10.1021/ac4014836 | Anal. Chem. 2013, 85, 10149–10158

and the WT-αHL nanopore results in larger blockades and longer dwell times, suggesting a stronger interaction. It appears that van der Waals forces between the longer hydrophobic OT ligands and the hydrophobic residues lining the inner surface of the protein cap (Supporting Information, Figure S-1, bottom panel) dominate this interaction and result in stronger binding. We also hypothesize that the OT ligands may also be able to interact with hydrophobic residues in the stem,[54] in the region just below the constriction, further strengthening the interaction. Another possible explanation for this observation was raised during the reviewing process. The assumption until now has been that the interaction between WT-αHL and MPSA NPs is attractive, based upon the electrostatic interaction between Lys147 (positively charged)and the sulfonate ligands (negative) and that Glu111 (negative) modulates this interaction. However, the opposite could also be true; Glu111 could repel the sulfonate ligands and Lys147 would modulate this repulsion. Under these circumstances, interactions with the MPSA/OT particles would be favored, resulting in larger current blockades and longer dwell times.

For the interaction between all types of NPs and the E111A mutant, we observe higher current blockade values compared with those observed for the WT-αHL (83−100% versus 17−29%). We attribute this difference to the fact that the interaction of the NP with the pore is dominated by the electrostatic interactions between sulfonate-terminated ligands and Lys147 residues. As predicted earlier, the OT ligands interfere with the ability of MPSA ligands to interact with Lys147 residues, hence MPSA/OT NPs exhibit a slight decrease in current blockade level and a decrease in dwell time when compared to MPSA NPs

The dwell time of NPs, in the WT-αHL nanopore, increases with applied potential. The increased stability of NPs within the protein cavity is likely due to the increased strength of the electrical field. At the same time, the electroosomotic flow of water through the slightly anion selective WT-αHL nanopore, from the cis to the trans side of the bilayer, is enhanced as the applied positive potential is increased, also contributing to the increased dwell time.[55] The dwell time of the interaction between the NPs and the E111A mutant nanopore decreases with the applied potential. According to previous theoretical studies,[56,57] it is expected that an increase in the local NP density in the region surrounding the nanopore results in a decrease in the dwell time. Put more simply, NPs are electrophoresed toward the nanopore and the lipid membrane in which it is contained. The increased local NP concentration in the region around the nanopore limits the capture rate due to the resulting inter-NPs collisions and repulsion, since only one NP can be captured at a time.[58] This effect is enhanced at higher applied potential (this effect will presumably occur for the WT-αHL nanopore as well, but it is overcome by the effect of the increased electrical field and increased electroosmotic flow). Furthermore, the E111A mutant is more anion selective,[59] resulting in a higher flow of anions through the pore which also increases with applied potential. The combination of these two effects overwhelms the effects of the increased electrical field and increased electroosmotic flow, resulting in a dwell time that decreases with increasing applied potential.

NPs are typically heterogeneous in size, morphology, ligand shell composition, and distribution.[60] Therefore each individual NP has a specific size, morphology, ligand shell composition, and distribution of ligands across its surface. The signature provided by the current blockade and duration of the individual interaction event depends upon all of these NP characteristics. Here, we focused mainly on the NPs' ligand shell composition and arrangement. It is interesting to look at each individual event, for each NP preparation, at a given applied potential, for both the WT-αHL and E111A mutant nanopores (Supporting Information, Figure S-2). We assume that there is overlap between MPSA/OT populations with the existence of similar ligand composition and arrangement in both MPSA:OT 2:1 and MPSA:OT 1:2 NP preparations that result in similar interaction with the protein nanopore. However, it is apparent that there are areas where signals do not overlap. Values that fall into these nonoverlapping regions can be used to precisely identify a specific NP preparation. Furthermore, values that fall into these nonoverlapping regions could be used to estimate the composition of a mixture of NP preparations. This can clearly be seen in the results presented here. The values that arise from the MPSA:OT 2:1 NPs type are found in the overlap region between the values from MPSA NPs and the MPSA:OT 1:2 NPs types. Finally, an individual signal that falls into the overlapping region cannot be precisely identified; however, on the basis of the blockade level and dwell time, a probability that it belongs to specific NP type can be assigned.

Only MPSA/OT NPs were able to cause permanent current blockades. The current blockade distribution is presented in Figure S-5 (Supporting Information). Representative traces from these permanent current blockade events are shown in Figure S-6 (Supporting Information). Permanent current blockades are defined as blockades that persist from when they occur until the end of the recording (up to 120 s). The blockade level of the permanent events is, as already discussed for the transient events, likely to be related to the specific NP captured from within the NP sample, with particular physical characteristics (e.g., size, ligand shell ratio, and arrangement). We attribute these permanent blockades to the fact that the OT ligand is longer than the MPSA ligand, thus NPs containing OT ligands are slightly larger and can be physically trapped inside the cavity of the cap domain. The larger OT-containing NPs are forced into the cavity as a result of the applied potential. Once inside the cavity, these NPs remain trapped until the polarity of the applied potential is reversed.[61] The ligand shell arrangement may also be of particular importance. Previous studies on similar NPs suggested a structured ligand shell, where phase separation among the ligands occurs into ordered, stripe-like domains, or "ripples".[43,62,63] Alternatively, other arrangements of ligands such as those found in Janus or "patchy" NPs are possible (reviewed in ref 64). Furthermore it has been demonstrated that the arrangement of the ligand shell depends on the size of the gold core.[65] Populations of NPs with gold core sizes between ∼1.5 and ∼3 nm are believed to possess mixed morphologies of Janus and striped NPs.[66] The diversity on NP ligand shell arrangement contributes to the variations in current blockade values and patterns observed for both the transient and permanent events.

In general, when interacting with the WT-αHL nanopore, the MPSA:OT 2:1 NPs cause higher current blockades than the MPSA:OT 1:2 NPs. Conversely, when interacting with the E111A mutant nanopore, the MPSA:OT 1:2 NPs seem to generate a higher current blockades. These results suggest that a stronger or more favored interaction exists between the MPSA:OT 2:1 NPs and the WT-αHL nanopore and between the MPSA:OT 1:2 NPs and the E111A nanopore. In the WT-αHL nanopore, since the interaction with the NPs depends

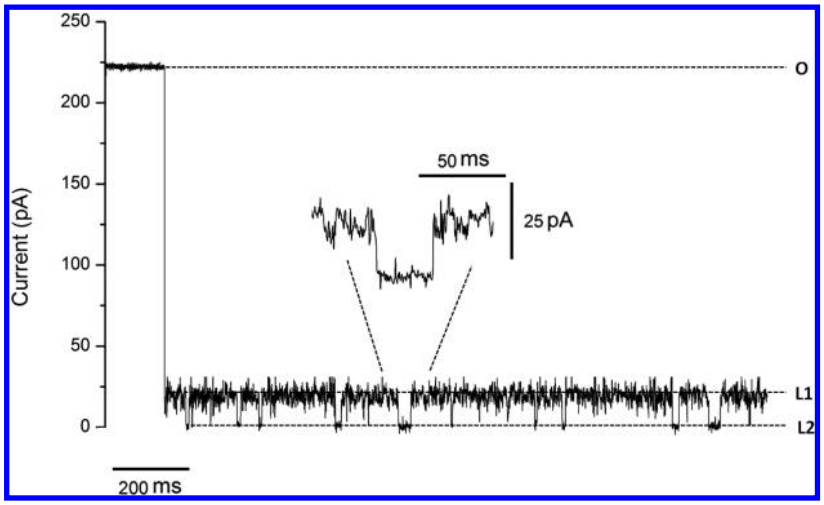

Figure 3. Representative capture event showing the ionic current signature produced by a single MPSA:OT 2:1 captured in the E111A mutant protein nanopore. Open pore current (level O) shows a sharp decrease, indicating the capture of a NP. Ionic current is impeded by the captured NP in a characteristic blockade pattern that contains two current levels (L1 and L2), between which the ionic current transitions, with duration (τ_{off}) of 4 ms. Here, the upper level, L1, corresponds to a ~91% blockade and the lower level, L2, to a ~99% blockade (relative to the open pore current). Recordings were made at +100 mV, in 2 M KCl, 10 mM HEPES (pH 8.0), in the presence of 10 μg mL^{-1} MPSA:OT 2:1 added on the cis side of the lipid bilayer.

mainly on the electrostatic interactions between Lys147 and the MPSA ligands, we assume that a higher contents of OT ligand hampers this interaction since relatively fewer MPSA ligands are available to interact and also because OT is a longer ligand. In the E111A mutant nanopore, the interaction with the NPs is still mainly electrostatic. However, as mentioned above, a higher increased local NP concentration is predicted to occur in the region around the nanopore, enhancing electrostatic repulsion between charged NPs and, thus, rendering the interaction between the NP and the nanopore less stable. This effect will be greater with a higher content of charged MPSA ligands, whereas the neutral, more hydrophobic OT ligands will attenuate this effect.

Some of these current permanent blockades present short-lived current amplitude changes (spikes) that we assign to movements or "fluctuations" of the MPSA/OT NP that is trapped inside the cavity of the cap domain. Another typical pattern observed was clear and discrete minor changes in current amplitude (rectangular events; Figure 3), leading to characteristic ionic current signatures.

Similar ionic current patterns, produced by single DNA hairpin molecules[67−69] and by an antimicrobial peptide[54] captured in the WT-αHL nanopore have already been described and interpreted. Previously, we also observed that, when a single MPSA NP was trapped in the WT-αHL protein cavity, at pH 8.0, the blockade level of the capture event showed minor changes in current amplitude.[25] We assigned these signatures to exchanges of electrostatic interactions between individual Lys147 residues, Glu111 residues, and the sulfonate ligand present at the surface of MPSA NPs. These small amplitude changes are not observed when a MPSA NP is captured by an E111A mutant nanopore. When a single MPSA/OT NP is captured and trapped in an E111A mutant nanopore, small changes in current amplitude are observed in the blockade level of the event (Figure 3). Having a heterogeneous composition, with both charged (sulfonate ligands) and noncharged ligands (OT ligands), MPSA/OT NPs are likely to form temporary electrostatic interactions between individual Lys147 residues and individual sulfonate ligands. The presence of OT ligands interferes with the ability of the NP to reach a stable interaction in which all Lys147 residues are bound to sulfonate ligands. Instead, we hypothesize that these current amplitude changes are due to breaking and reforming of individual electrostatic interactions between the Lys147 residue at the constriction region of the E111A protein and the sulfonate ligand of the MPSA/OT NPs. Alternatively, these amplitude changes could be due to the breaking and reforming of van der Waals forces between OT ligands and hydrophobic residues within the cavity or just below the constriction region. For specific MPSA/OT preparations and at certain applied potentials, the small amplitude changes were observed in more than one permanent event. Analysis of the blockade levels (L1 and L2, in Figure 3) and dwell time within each permanent event reveals that, even for the same NP preparation at the same applied potential, differences in these two parameters are observed (Supporting Information, Figure S-7). We assume that each permanent event corresponds to a single trapped NP. These differences in blockade level and dwell time suggest that the individual trapped NPs differ in their physical characteristics (e.g., size, ligand shell ratio, and arrangement). We believe that these particular ionic current signatures reveal further insights on the molecular interaction between NPs and the nanopore and, thus, can be used to describe each individually captured NP.

■ CONCLUSIONS

Organic monolayer protected NPs are promising materials for a wide range of applications. However, NP research lacks a single platform that can quickly and easily measure variation of NPs within a heterogeneous mixture (either single or multiple ligands). Here, we have presented a pioneering study based on the use of the biological nanopores WT-αHL and its E111A mutant, for the detection of, and discrimination between, differently modified gold-NPs. Analysis of a population of NPs is, generally, based on bulk analysis methods (such as analytical ultracentrifugation and dynamic light scattering). The method discussed here, a single molecule analysis using the biological nanopore αHL as a sensor, assesses NPs on an individual basis.

Using this method, it was not possible to assign a precise value for current blockade or dwell time to each type of NP. Instead, for each NP type, we observe a characteristic range of current blockades and dwell times centered around a median value with a characteristic spread. We have observed that the MPSA/OT preparations are more heterogeneous than the MPSA preparation. We assume that the heterogeneity found in MPSA/OT NP preparations arises from differences in size, ligand composition, and ligand arrangement. Furthermore we assume that there is overlap between the MPSA/OT NP preparations and that NPs of similar ligand composition and arrangement exist in both MPSA:OT 2:1 and MPSA:OT 1:2 NP preparations. These characteristics appear to be reflected in our results, since MPSA NPs have a more defined blockade level and dwell time with a more confined spread of values. For the MPSA/OT NPs, the blockade levels and dwell times are not centered on a particular value and there appears to be a much greater spread for both parameters. The overlap between the populations is also interesting; blockade levels and dwell times for the MPSA:OT 2:1 NPs are found between the values obtained for MPSA and MPSA:OT 1:2 NPs. It is very tempting to assume that the overlap and range of values reflects physical characteristics and the degree of homo/heterogeneity. However, supplementary studies, and perhaps different methodologies, are necessary in order to confirm this hypothesis. This is because it is possible that all of the features described here, blockade levels, dwell times, spread of values, and overlap of values, are just characteristic of the NPs being analyzed: the differing spreads for blockade level and dwell times, and overlap between them, would thus simply be a coincidence. This uncertainty means that for a direct, quantitative assessment of a NP population using this method, further improvements are needed. In the meantime, this method can be used compare different batches of NPs or to compare a specific batch of NPs to an existing range of standards, making this a very useful tool with which to perform quality control on NP preparations.

■ ASSOCIATED CONTENT

Supporting Information

Additional information and results as noted in the text. This material is available free of charge via the Internet at http://pubs.acs.org.

■ AUTHOR INFORMATION

Corresponding Author

*E-mail: elisacampos@itqb.unl.pt. Fax: +351 21 441 12 77.

Present Address

[‖]Y.A.: IBM Watson Research Center, Yorktown Heights, NY.

Author Contributions

The manuscript was written through contributions of all authors. All authors have given approval to the final version of the manuscript.

Notes

The authors declare no competing financial interest.

■ ACKNOWLEDGMENTS

This work was supported by Fundação para a Ciência e a Tecnologia (FCT) through Grant PEst-OE/EQB/LA0004/2011 and Project PTDC/QUI-QUI/099599/2008. E.C. was financially supported by the FCT PhD Studentship SFRH/BD/40431/2007. J.Y. was financially supported by the FCT Post Doc Fellowship SFRH/BPD/80071/2011.

■ REFERENCES

(1) Griffiths, J. *Anal. Chem.* **2008**, *80*, 23−27.
(2) Howorka, S.; Siwy, Z. *Chem. Soc. Rev.* **2009**, *38*, 2360−2384.
(3) Majd, S.; Yusko, E. C.; Billeh, Y. N.; Macrae, M. X.; Yang, J.; Mayer, M. *Cur. Opin. Biotechnol.* **2010**, *21*, 439−476.
(4) Maitra, R. D.; Kim, J.; Dunbar, W. B. *Electrophoresis* **2012**, *33*, 3418−3428.
(5) Braha, O.; Gu, L. Q.; Zhou, L.; Lu, X.; Cheley, S.; Bayley, H. *Nat. Biotechnol.* **2000**, *18*, 1005−1007.
(6) Guan, X.; Gu, L. Q.; Cheley, S.; Braha, O.; Bayley, H. *ChemBioChem* **2005**, *6*, 1875−1881.
(7) Wang, D.; Zhao, Q.; Zoysa, R. S. S. d.; Guan, X. *Sens. Actuators, B: Chem.* **2009**, *139*, 440−446.
(8) Gu, L. Q.; Braha, O.; Conlan, S.; Cheley, S.; Bayley, H. *Nature* **1999**, *398*, 686−690.
(9) Boersma, A. J.; Bayley, H. *Angew. Chem., Int. Ed.* **2012**, *51*, 9606−9609.
(10) Wang, H. Y.; Ying, Y. L.; Li, Y.; Kraatz, H. B.; Long, Y. T. *Anal. Chem.* **2011**, *83*, 1746−1752.
(11) Movileanu, L. *Trends Biotechnol.* **2009**, *27*, 333−341.
(12) Wang, Y.; Zheng, D.; Tan, Q.; Wang, M. X.; Gu, L. Q. *Nat. Nanotechnol.* **2011**, *6*, 668−74.
(13) Bayley, H.; Luchian, T.; Shin, S.-H.; Steffensen, M. In *Single Molecules and Nanotechnology*; Rigler, R., Vogel, H., Eds.; Springer: Berlin Heidelberg, Germany, 2008; Vol. *12*, pp 251−277.
(14) McGinn, S.; Gut, I. G. *Nat. Biotechnol.* **2013**, *30*, 366−372.
(15) Ma, L.; Cockroft, S. L. *ChemBioChem* **2010**, *11*, 25−34.
(16) Wang, H.-Y.; Ying, Y.-L.; Li, Y.; Long, Y.-T. *Chem. Asian J.* **2010**, *5*, 1952−1961.
(17) Misakian, M.; Kasianowicz, J. J. *J. Membr. Biol.* **2003**, *195*, 137−146.
(18) Menestrina, G. *J. Membr. Biol.* **1986**, *90*, 177−190.
(19) Kang, X.-f.; Gu, L.-Q.; Cheley, S.; Bayley, H. *Angew. Chem., Int. Ed.* **2005**, *44*, 1495−1499.
(20) Krasilnikov, O. V.; Rodrigues, C. G.; Bezrukov, S. M. *Phys. Rev. Lett.* **2006**, *97*, 018301.
(21) Pastoriza-Gallego, M.; Oukhaled, G.; Mathé, J.; Thiebot, B.; Betton, J.-M.; Auvray, L. c.; Pelta, J. *FEBS Lett.* **2007**, *581*, 3371−3376.
(22) Jayawardhana, D. A.; Crank, J. A.; Zhao, Q.; Armstrong, D. W.; Guan, X. *Anal. Chem.* **2009**, *81*, 460−464.
(23) Song, L. Z.; Hobaugh, M. R.; Shustak, C.; Cheley, S.; Bayley, H.; Gouaux, J. E. *Science* **1996**, *274*, 1859−1866.
(24) Bayley, H.; Jayasinghe, L. *Mol. Membr. Biol.* **2004**, *21*, 209−220.
(25) Campos, E.; Asandei, A.; McVey, C. E.; Dias, J. C.; Oliveira, A. S. F.; Soares, C. M.; Luchian, T.; Astier, Y. *Langmuir* **2012**, *28*, 15643−15650.
(26) Giljohann, D. A.; Seferos, D. S.; Daniel, W. L.; Massich, M. D.; Patel, P. C.; Mirkin, C. A. *Angew. Chem., Int. Ed.* **2010**, *49*, 3280−3294.
(27) Salata, O. *J. Nanobiotechnol.* **2004**, *2*, 3.
(28) Tiwari, P.; Vig, K.; Dennis, V.; Singh, S. *Nanomaterials* **2011**, *1*, 31−63.
(29) Nie, Z. H.; Petukhova, A.; Kumacheva, E. *Nat. Nanotechnol.* **2010**, *5*, 15−25.
(30) Falabella, J. B.; Cho, T. J.; Ripple, D. C.; Hackley, V. A.; Tarlov, M. J. *Langmuir* **2010**, *26*, 12740−12747.
(31) Kang, X.-f.; Cheley, S.; Rice-Ficht, A. C.; Bayley, H. *J. Am. Chem. Soc.* **2007**, *129*, 4701−4705.
(32) White, R. J.; Ervin, E. N.; Yang, T.; Chen, X.; Daniel, S.; Cremer, P. S.; White, H. S. *J. Am. Chem. Soc.* **2007**, *129*, 11766−11775.
(33) Shim, J. W.; Gu, L. Q. *Anal. Chem.* **2007**, *79*, 2207−2213.
(34) Mohammad, M. M.; Movileanu, L. In *Nanopore-Based Technology*; Gracheva, M. E., Ed.; Springer Science+Business Media LLC: New York, 2012; pp 21−37.
(35) Lin, J. C.; Chuang, W. H. *J. Biomed. Mater. Res.* **2000**, *51*, 413−423.
(36) Shen, C. H.; Lin, J. C. *Colloids Surf. B: Biointerfaces* **2010**, *79*, 156−163.
(37) Maglia, G.; Heron, A. J.; Stoddart, D.; Japrung, D.; Bayley, H. *Methods Enzymol.* **2010**, *475*, 591−623.

(38) Schrödinger, LLC. *The PyMOL Molecular Graphics System*, version 1.4.1, 2011.
(39) Rincon-Restrepo, M.; Mikhailova, E.; Bayley, H.; Maglia, G. *Nano Lett.* **2011**, *11*, 746−750.
(40) McVey, C. E.; Walsh, M. A.; Dodson, G. G.; Wilson, K. S.; Brannigan, J. A. *J. Mol. Biol.* **2001**, *313*, 139−150.
(41) Brust, M.; Walker, M.; Bethell, D.; Schiffrin, D. J.; Whyman, R. *J. Chem. Soc. Chem. Comm.* **1994**, 801−802.
(42) Kang, S. Y.; Kim, K. *Langmuir* **1998**, *14*, 226−230.
(43) Centrone, A.; Hu, Y.; Jackson, A. M.; Zerbi, G.; Stellacci, F. *Small* **2007**, *3*, 814−817.
(44) Carney, R. P.; Kim, J. Y.; Qian, H.; Jin, R.; Mehenni, H.; Stellacci, F.; Bakr, O. M. *Nat. Commun.* **2011**, *2*, 335.
(45) Montal, M.; Mueller, P. *Proc. Natl. Acad. Sci. U.S.A.* **1972**, *69*, 3561−3566.
(46) Jadzinsky, P. D.; Calero, G.; Ackerson, C. J.; Bushnell, D. A.; Kornberg, R. D. *Science* **2007**, *318*, 430−433.
(47) Colquhoun, D. In *Microelectrode Techniques: The Plymouth Workshop Handbook*; Odgen, D. C., Ed.; Company of Biologists Limited: Cambridge, U.K., 1994; pp 101−139.
(48) Ying, Y. L.; Li, D. W.; Li, Y.; Lee, J. S.; Long, Y. T. *Chem. Commun.* **2011**, *47*, 5690−5692.
(49) Dawson, B.; Trapp, R. G., *Basic & Clinical Biostatistics*, 4 ed.; McGraw-Hill: New York, 2004.
(50) Manikandan, S. *J. Pharmacol. Pharmacother.* **2011**, *2*, 315−316.
(51) Mcgill, R.; Tukey, J. W.; Larsen, W. A. *Am. Stat.* **1978**, *32*, 12−16.
(52) Astier, Y.; Uzun, O.; Stellacci, F. *Small* **2009**, *5*, 1273−1278.
(53) Maglia, G.; Restrepo, M. R.; Mikhailova, E.; Bayley, H. *Proc. Natl. Acad. Sci. U.S.A.* **2008**, *105*, 19720−19725.
(54) Asandei, A.; Apetrei, A.; Park, Y.; Hahm, K. S.; Luchian, T. *Langmuir* **2011**, *27*, 19−24.
(55) Asandei, A.; Mereuta, L.; Luchian, T. *J. Phys. Chem. B* **2011**, *115*, 10173−10181.
(56) Bauer, W. R.; Nadler, W. *Proc. Natl. Acad. Sci. U.S.A.* **2006**, *103*, 11446−11451.
(57) Kasianowicz, J. J.; Nguyen, T. L.; Stanford, V. M. *Proc. Natl. Acad. Sci. U.S.A.* **2006**, *103*, 11431−11432.
(58) Henrickson, S. E.; Misakian, M.; Robertson, B.; Kasianowicz, J. J. *Phys. Rev. Lett.* **2000**, *85*, 3057−3060.
(59) Noskov, S. Y.; Im, W.; Roux, B. *Biophys. J.* **2004**, *87*, 2299−2309.
(60) You, C.-C.; Chompoosor, A.; Rotello, V. M. *Nano Today* **2007**, *2*, 34−43.
(61) Kasianowicz, J. J.; Brandin, E.; Branton, D.; Deamer, D. W. *Proc. Natl. Acad. Sci. U.S.A.* **1996**, *93*, 13770−13773.
(62) Jackson, A. M.; Hu, Y.; Silva, P. J.; Stellacci, F. *J. Am. Chem. Soc.* **2006**, *128*, 11135−11149.
(63) Uzun, O.; Hu, Y.; Verma, A.; Chen, S.; Centrone, A.; Stellacci, F. *Chem. Commun. (Cambridge, U.K.)* **2008**, 196−198.
(64) Lattuada, M.; Hatton, T. A. *Nano Today* **2011**, *6*, 286−308.
(65) Carney, R. P.; DeVries, G. A.; Dubois, C.; Kim, H.; Kim, J. Y.; Singh, C.; Ghorai, P. K.; Tracy, J. B.; Stiles, R. L.; Murray, R. W.; Glotzer, S. C.; Stellacci, F. *J. Am. Chem. Soc.* **2007**, *130*, 798−799.
(66) Kim, H.; Carney, R. P.; Reguera, J.; Ong, Q. K.; Liu, X.; Stellacci, F. *Adv. Mater.* **2012**, *24*, 3857−3863.
(67) Winters-Hilt, S.; Vercoutere, W.; DeGuzman, V. S.; Deamer, D.; Akeson, M.; Haussler, D. *Biophys. J.* **2003**, *84*, 967−976.
(68) Vercoutere, W. A.; Winters-Hilt, S.; DeGuzman, V. S.; Deamer, D.; Ridino, S. E.; Rodgers, J. T.; Olsen, H. E.; Marziali, A.; Akeson, M. *Nucleic Acids Res.* **2003**, *31*, 1311−1318.
(69) DeGuzman, V. S.; Lee, C. C.; Deamer, D. W.; Vercoutere, W. A. *Nucleic Acids Res.* **2006**, *34*, 6425−6437.